Semnan University

Mechanics of Advanced Composite Structures

journal homepage: http://MACS.journals.semnan.ac.ir

Buckling analysis of FML cylindrical shells under combined axial and torsional loading

A.R. Ghasemi, S. Kiani, A. Tabatabaeian

Composite and Nanocomposite Research Laboratory, Department of Solid Mechanic, Faculty of Mechanical Engineering, University of Kashan, Kashan, Iran

KEYWORDS

Fiber metal laminates (FMLs)
Cylindrical shell
Buckling analysis
Finite element method (FEM)
Torsional buckling

ABSTRACT

Generally, in-served cylindrical shells buckling usually takes place not merely under one of the basic loads, i.e., axial compression, lateral pressure, and torsion, but under a combination of them. The buckling behavior of fiber-metal laminate (FML) cylindrical shells under combined axial and torsional loading is studied in this paper. The Kirchhoff Love-type assumption is employed to study the axial buckling load. Then, an extended finite element (FE) model is presented and results are compared. A number of consequential parameters such as lay-up arrangement, metal type and metal volume fraction are employed and enhancement of buckling behavior of the shell is also studied. Finally, the interaction of axial /torsional loading is analyzed and discussed. The results show that as the metal volume fraction rises to 15%, the endurable buckling load increases almost 43% more than the state in which there is no metal layer. The numerical results show that increasing the metal volume percentage leads to a decrease in buckling performance of the structure under axial loading.

1. Introduction

Due to the growth of application of shell type structures such as buildings, space vehicles, submarines and storage tanks, interest in the stability of shells has similarly increased by researchers and engineers. [1–4]. The paradoxical behavior of buckling load of cylindrical shells under axial compression is a long-standing problem in structural mechanics. [5-8]. A lot of investigation has already been carried out on this phenomenon. For example, Geier et al. [9] studied the influence of laminate stacking on the buckling of composite cylindrical shells subjected to axial compression. They proposed analytical and semi-analytical methods to predict the buckling loads and compared them with experimental results. It was shown that the buckling loads of laminated cylinders strongly depended on the position of the differently oriented layers within the shell. Tafreshi and Bailey. [10] investigated the instability of imperfect composite cylindrical shells under combined loading. They proved that the effects of imperfections were more apparent when the composite cylindrical shells were subject to combined loadings. The results showed that the buckling and non-linear response of geometrically imperfect shell structures subjected to complex loading conditions may not be characterized correctly by an elastic linear bifurcation buckling analysis. In other research by Taheri et al. [11], buckling behavior of composite cylinders with cutout was analyzed numerically and experimentally. Numerical analyses were performed for three different groups of the perforated cylinders to evaluate the effect of the growing cutout size on the buckling behavior. The results confirmed that cutout effect was dominant, for the cylinder under consideration, so considering initial geometric imperfection had a negligible effect on the predicted buckling load. In a recent study, Shen and Xiang [12] also presented a comprehensive study on the post buckling of functionally graded graphene-reinforced composite laminated cylindrical shells subjected to external pressure in thermal environments.

* Corresponding author. Tel.: +98-31-55912426; Fax: +98-31-55912424
E-mail address: Ghasemi@kashanu.ac.ir

DOI: 10.22075/MACS.2020.18521.1219
Received 2019-08-20; Received in revised form 2020-01-25; Accepted 2020-03-22

Application of novel materials can be seen as an effective way to control different mechanical behaviors such as buckling or stress of the structures [13–21]. One of the most remarkable materials is fiber metal laminates (FMLs) which has been widely used in engineering structures, recently. FMLs [22, 23] are hybrid materials which are composed of several thin metal layers and fiber reinforced epoxy composite layers. These laminates integrate the significant properties of metals such as high damage tolerance and ductility with great features of composite materials such as high fatigue resistance, weight-savings and specialized strength properties. For instance, Glare-FML has been widely employed in the aerospace industry in order to reduce the weight of aircraft. Moreover, FMLs possess more superior impact resistance than the conventional fiber-reinforced composite laminates (FRPs). Also, impact damage on FMLs would be easily visible to the naked eye, because of the visible deformation that remains on the impacted layer, where as it would be difficult to detect most impact induced damage in FRPs [24–26]. Banat et al. [27] discussed the buckling and post buckling behavior of thin walled FML profiles subjected to axial loading. The results of substantial experimental investigations were compared with FML panel/columns modelling in finite element analysis and with an analytical method based on Koiter's asymptotic theory. Detailed analysis was also performed to assess the influence of the various fiber alignments on the specimen's buckling and post buckling response. Asaee et al. [28] investigated the delamination buckling behavior of graphene Nano platelets (GNP) reinforced by 3D fiber-metal laminates (3DFMLs). In other research [29], they predicted the low-velocity impact response of 3D-fiber metal laminates using a practical analytical model. Many other researches have been performed about buckling behavior of various structures [30–32]. The objective of the present study is investigation of the buckling behavior of FML cylindrical shells under torsional and axial loading. All investigations are presented for two substances: FMLs and polymer matrix composites (PMCs). The analytical formulations are presented based on the Kirchhoff Love-type assumption to calculate the axial buckling load of cylinders. Subsequently, various stacking sequences are considered and the most desirable probable lay-up is chosen. The results are compared with the finite element method (FEM) analysis. Also, some noticeable parameters such as different metal types, various metal volume fractions and the mass of composite structures are considered and their influence is investigated. Lastly, the interaction state of axial and torsional loadings is studied and results are presented.

2. Analytical formulation

2.1. Problem description

A schematic of FML cylinder is shown in Fig. 1. As shown in this figure, the present structure consists of two metal layers at the inner and outer sides of the glass fiber reinforced polymer (GFRP) laminates.

Also, some necessary geometrical features are presented in Fig.1 in which L is length of the cylinder, t denoted the thickness and R is middle surface radius of the cylinder.

The analytical formulations are presented for pure axial compression. Then the FEM buckling behavior modeling is proposed for both axial and torsional loadings and the effects of interaction are numerically analyzed.

2.2. Kinematic relations

Based on shallow shell theory, the Kirchhoff Love-type assumption represents the distribution of strain over the thickness as [9]:

$$\varepsilon(x,y,z) = \varepsilon(x,y) - z\,\kappa \tag{1}$$

where $\kappa$is curvature and $\varepsilon(x,y)$is two-dimensional strain distribution in the reference surface. According to the above displacement field, the strain components for a cylindrical shell are expressed as [9]:

$$\varepsilon = \begin{Bmatrix} \varepsilon_x \\ \varepsilon_y \\ \gamma_{xy} \end{Bmatrix} = \begin{Bmatrix} \frac{\partial u}{\partial x} \\ \frac{\partial v}{\partial y} - \frac{w}{R} \\ \frac{\partial u}{\partial y} + \frac{\partial v}{\partial x} \end{Bmatrix} \tag{2}$$

$$\kappa = \begin{Bmatrix} \frac{\partial^2 w}{\partial x^2} \\ \frac{\partial^2 w}{\partial y^2} \\ \frac{2\,\partial^2 w}{\partial x\,\partial y} \end{Bmatrix} \tag{3}$$

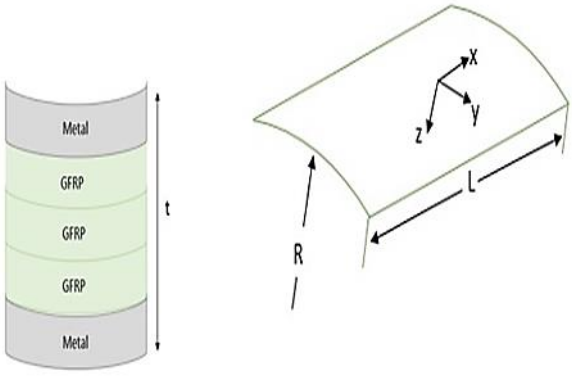

Fig. 1 Schematic of FML cylinder

where u, $v$and $w$are displacements in x, $y$and $z$directions, respectively.

The compatibility condition between the strain components could be written as [9]:

$$\frac{\partial^2 \varepsilon_x}{\partial y^2} + \frac{\partial^2 \varepsilon_y}{\partial x^2} - \frac{\partial^2 \gamma_{xy}}{\partial x\, \partial y} = -\frac{1}{R}\frac{\partial^2 w}{\partial x^2} \quad (4)$$

2.3. Governing equations

Axial forces and bending moments per unit length are:

$$N = \begin{Bmatrix} n_x \\ n_y \\ n_{xy} \end{Bmatrix} \qquad M = \begin{Bmatrix} m_x \\ m_y \\ m_{xy} \end{Bmatrix} \quad (5)$$

In order to achieve the equilibrium condition, the following three partial differential equations must be satisfied [9]:

$$\frac{\partial n_x}{\partial x} + \frac{\partial n_{xy}}{\partial y} = 0 \quad (6a)$$

$$\frac{\partial n_{xy}}{\partial x} + \frac{\partial n_y}{\partial y} = 0 \quad (6b)$$

$$\frac{\partial^2 m_x}{\partial x^2} + 2\frac{\partial^2 m_{xy}}{\partial x\, \partial y} + \frac{\partial^2 m_y}{\partial y^2} - \frac{1}{R}n_y - \hat{N}_x \frac{\partial^2 w}{\partial x^2} - \hat{N}_y \frac{\partial^2 w}{\partial y^2} = 0 \quad (6C)$$

in which n_x, n_y, n_{xy} and m_x, m_y, m_{xy} are the components of membrane forces and bending/twisting moments per unit length associated with buckling deflection, respectively. Also, $\hat{N}_x$and $\hat{N}_y$ are the membrane forces in general state and considered positive in tension. It should be noticed that since there is no buckling due to torsion, the term of shear membrane force $\hat{N}_{xy}$is considered zero in relations. The equations 6a and 6b are known as equilibriums of a plate under in-plane loads. Airy's stress function ϕ is represented in order to derive the membrane forces of the equations 6 as [9]:

$$\begin{cases} n_y = \frac{\partial^2 \phi}{\partial x^2} \\ n_{xy} = -\frac{\partial^2 \phi}{\partial y\, \partial x} \end{cases} \quad (7)$$

In order to apply the compatibility equilibrium (Eq. 4), the constitutive relations are developed. The stress-strain relation is presented as [33] :

$$\sigma_k = \bar{Q}_k \varepsilon_k \quad (8)$$

where $\bar{Q}$is stiffness matrix and k represents number of the layer.

Also, there are linear relations between the stress resultants (N and M) and the strain and change of curvature (ε and κ) as follows [34]:

$$\begin{cases} N = A\varepsilon + B\kappa \Rightarrow \varepsilon = A^{-1}(N - B\,\kappa) \\ M = B^T\varepsilon + D\kappa \Rightarrow M = B^T A^{-1} N + \\ \qquad (D - B^T\, A^{-1}\, B) \end{cases} \quad (9)$$

in which A, B and D are the in-plane stiffness matrix, the extension-bending coupling matrix and the bending stiffness matrix, respectively and defined as [9, 35]:

$$\begin{cases} A = \sum_{k=1}^{N} \bar{Q}_k (z_k - z_{k-1}) \\ B = -\frac{1}{2}\sum_{k=1}^{N} \bar{Q}_k ({z^2}_k - {z^2}_{k-1}) \\ C = -\frac{1}{3}\sum_{k=1}^{N} \bar{Q}_k ({z^3}_k - {z^3}_{k-1}) \end{cases} \quad (10)$$

where N is the total number of layers.

In this step, three parameters are introduced to rewrite equations 9 more concisely as:

$$\begin{cases} a = A^{-1} \\ e = A^{-1}B = aB \\ \bar{D} = D - B^T A^{-1} B \end{cases} \quad (11)$$

in which a, e and $\bar{D}$are the membrane compliance, eccentricity matrix and modified bending matrix, respectively. Therefore, equations 9 are expressed as:

$$\begin{cases} \varepsilon = aN - e\kappa \\ M = e^T N + \bar{D}\kappa \end{cases} \quad (12)$$

Substituting equations 3 and 12 into equations 4 and 6c results in two differential equations in terms of four parameters a, e, N and $\bar{D}$as follows:

$$a_{22}\frac{\partial^4 \phi}{\partial x^4} + (2a_{12} + a_{33})\frac{\partial^4 \phi}{\partial x^2\, \partial y^2} + a_{11}\frac{\partial^4 \phi}{\partial y^4} - [e_{21}\frac{\partial^4 w}{\partial x^4} + (e_{11} + e_{22} - 2\,e_{33})\frac{\partial^4 w}{\partial x^2\, \partial y^2} + e_{21}\frac{\partial^4 w}{\partial y^4} - \frac{1}{R}\frac{\partial^2 w}{\partial x^2}] = 0 \quad (13)$$

$$\bar{D}_{11}\frac{\partial^4 w}{\partial x^4} + 2(\bar{D}_{12} + 2\bar{D}_{33})\frac{\partial^4 w}{\partial x^2\, \partial y^2} + \bar{D}_{22}\frac{\partial^4 w}{\partial y^4} - \hat{N}_x\frac{\partial^2 w}{\partial x^2} - \hat{N}_y\frac{\partial^2 w}{\partial y^2} + [e_{21}\frac{\partial^4 \phi}{\partial x^4} + (e_{11} + e_{22} - 2\,e_{33})\frac{\partial^4 \phi}{\partial x^2\, \partial y^2} + e_{21}\frac{\partial^4 \phi}{\partial y^4} - \frac{1}{R}\frac{\partial^2 \phi}{\partial x^2}] = 0 \quad (14)$$

3. Solution procedure

To satisfy the simply-supported boundary condition of cylindrical shell which is [9]:

$$\begin{cases} m_x = 0 \\ n_x = 0 \\ w = 0 \\ \vartheta = 0 \end{cases} \quad (15)$$

The following solution is proposed for buckling modes of the cylindrical shell [9]:

$$w = C_1\, sin\, \beta\, x\, cos\, \eta\, y \quad (16)$$

$$\phi = C_2\, sin\, \beta\, x\, cos\, \eta\, y \quad (17)$$

in which β and η are introduced as:

$$\begin{cases}\beta = \frac{m\pi}{L} \\ \eta = \frac{n}{R}\end{cases} \quad (18)$$

Note that $m$is the number of axial half-waves and$n$is the number of complete circumferential waves of the buckling mode.

For pure axial compression, the buckling load is evaluated as [9]:

$$N_i = \frac{1}{\beta^2}\left\{\bar{D}_{11}\beta^4 + 2(\bar{D}_{12} + 2\bar{D}_{33})\beta^2\eta^2 + \bar{D}_{22}\eta^4 + \frac{[e_{21}\beta^4+(e_{11}+e_{22}-2e_{33})\beta^2\eta^2+e_{12}\eta^4+\beta^2/R]^2}{a_{22}\beta^4+(2a_{12}+a_{33})\beta^2\eta^2+a_{11}\eta^4}\right\} \quad (19)$$

It can be written in terms of the components in x and y directions as:

$$\begin{cases}\widehat{N}_X = -N_i \\ \widehat{N}_y = 0\end{cases} \quad (20)$$

Then, the critical axial buckling load which is the smallest positive amount of N_i, can be derived for any combination of axial half-waves m and circumferential waves n:

$$\widehat{N}\, N_i)_{xcr} \quad (21)$$

4. FEM buckling behavior modeling

A numerical simulation is carried out using the Abaqus commercial software packages. A static displacement-controlled analysis is used to derive the critical values and load displacement curves for the cases under study. The mesh elements chosen for the finite element analysis are S4R shell elements. This is a 4-node linear element with reduced integration. Approximate element sizes considered in the analysis are 5mm in length.

The boundary conditions are simply supported at both sides of the cylinder. Therefore, displacement vectors were set to zero at the edges of the cylinder. The torsion moment and axial loading are uniformly distributed along the acting edge. Fig. 2 shows the buckling mode shape of various stacking sequences.

5. Numerical results and discussion

The numerical results of our problem are presented in this section. Before presentation of full numerical results, some necessary geometrical and mechanical characteristics are presented in Table.1:

5.1. Validation

The present results are compared using comparison with literature results presented by Geier et al. [9]. They investigated the axial buckling load of a composite cylinder with stacking sequence of with no metal layers. As shown in Fig.3, our results approached the results from Geier et al. [9] as the metal volume fraction is equal to 0%. There is reasonable agreement and the error is less than 3%.

5.2. Study of various metal types and their volume fractions

Various stacking sequences are investigated in this section. The presented formulation in the previous part has been used to determine the critical axial buckling load of different stacking sequences and the results are compared to FEM results. Also, the error between two methods and buckling mode shape of each lay-up are presented in Table.2. It should be noticed that all calculations have been carried out considering the laminate stacking from inner to outer ply. As shown in Table.2, the and lay-ups can tolerate the most axial buckling loads. Study of mode shapes revealed that the cases with a twisting mode shape showed a higher error percentage.

Based on the buckling load and error of various lay-ups presented in Table.2, the is the optimal lay-up. Therefore, this stacking sequence is employed for next sections.

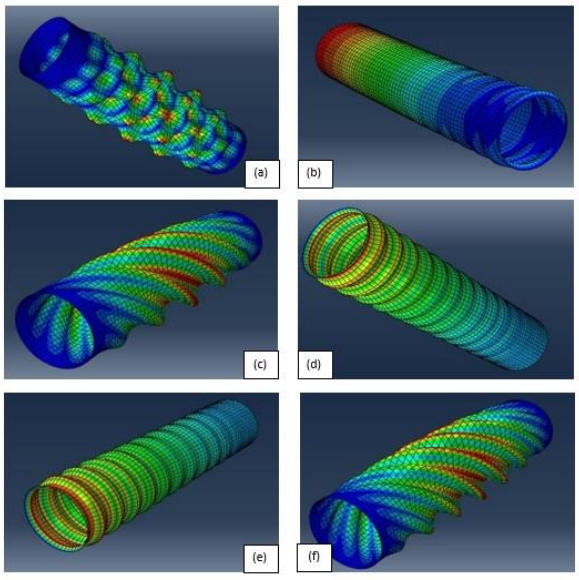

Fig. 2 The FEM results of the first axial buckling mode shape for various stacking sequences:
a)$[0/90]_6$, b)$[\pm45/(0/90)_5]$,
c)$[(0/90)_5/\pm45]$,d)$[(\pm45)_2/(0/90)_4]$,
e) $[(0/90)_4/(\pm45)_2]$, f) $[\pm45]_6$

Table.1: Geometrical and mechanical characteristics

Geometrical properties		Material	Mechanical properties
R (mm)	125	Al2024	E= 73.1 GPa, $\vartheta = 0.33$
L (mm)	1000	Ti6Al4V	E= 110 GPa, $\vartheta = 0.31$
t (mm)	3	Az91	E= 45 GPa, $\vartheta = 0.35$

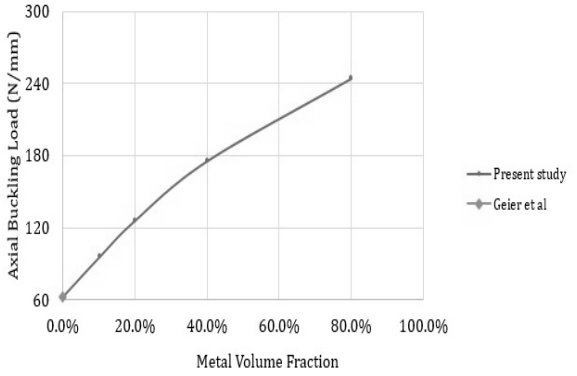

Fig. 3 Comparison of present study with Geier et al. [9]

Table.2: Axial buckling load of various stacking sequences calculated with two methods

Lay-up	Analytical solution	FEM	Error
$[0/90]_6$	618.5	666.1	7.1%
$[\pm45/(0/90)_5]$	728.6	799.7	8.9%
$[(0/90)_5/\pm45]$	728.5	667.0	8.11%
$[(\pm45)_2/(0/90)_4]$	795.8	701.3	11.8%
$[(0/90)_4/(\pm45)_2]$	779.4	672.7	13.6%
$[\pm45]_6$	601.5	614.2	2.1%

5.3. Study of various metal types and their volume fractions

The effects of addition of metal layers are studied in this section. Three metals including Ti6Al4V, Az91 and Al2024 are considered to be investigated in this study. These particular metals have been chosen due to their wide application in the aviation industry and also their appropriate qualities. Furthermore, availability and cost are two other parameters which approved the selection of these three metal types [36–38]. Figures 4 and 5 show the axial and torsional buckling load of various metals, respectively. As presented by these figures, Ti6Al4v outperforms the other metals in both axial and torsional loadings. The results of Al2024 is close to Ti6Al4v. It is observed that PMCs endure noticeably less buckling load than FMLs.

Table 3 shows the mass and the critical load to mass ratio ($\frac{N_c}{m}$and $\frac{T_c}{m}$) of various metals. The presented calculations show that Ti6Al4V has the highest critical load to mass ratio. It can also be concluded that addition of Az91 increases the critical load to mass ratio without increasing the mass. Furthermore, the critical load to mass ratio of the Al2024 is close to Ti6Al4V while being more available and economical.

According to the presented information about availability and sustainable buckling loads, one might conclude overall, that the Al2024 is the best choice among the mentioned materials.

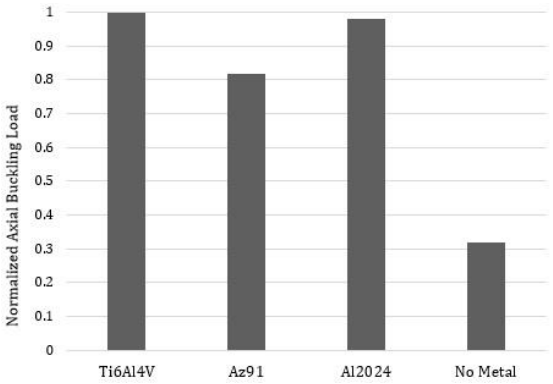

Fig. 4 Comparison of axial buckling load of various metal types

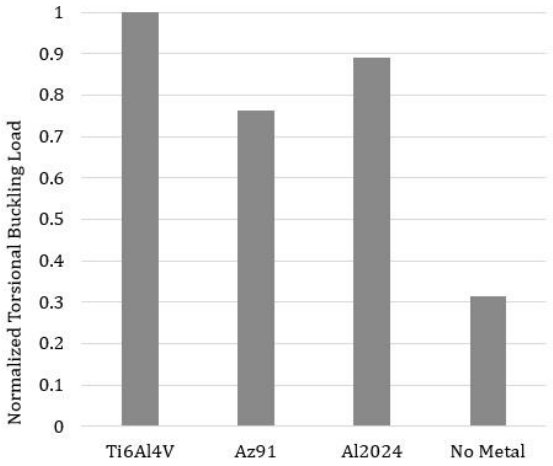

Fig. 5 Comparison of torsional buckling load of various metal types

Table.3: Comparison of the mass and critical load to mass ratio of various metal types

	Mass (gr)	N_c/m	T_c/m
Non-FML	4.24	188.60	$3.56\text{x}10^6$
Al2024	4.95	379.89	$7.68\text{x}10^6$
Ti6Al4V	6.37	386.97	$8.63\text{x}10^6$
Az91	4.24	317.21	$6.58\text{x}10^6$

Figures 6 and 7 demonstrate the axial and torsional buckling load in terms of metal volume fraction. Regarding previous analyses, the lay-up is considered. As depicted by these figures, addition of metal layers enhances the buckling behavior of composite structures greatly.

The efficiency of addition of metal layers is more noticeable when the metal volume fraction is less than 15%. It is proved that as the metal volume fraction rises to 15%, the endurable buckling load increases almost 43% more than the state where there is no metal layer. Also, it is observed that the torsional loading has the same behavior as axial loading when metal layers are added. Therefore, the usage of appropriate amounts of metals may efficiently improve the buckling stability of composite shells.

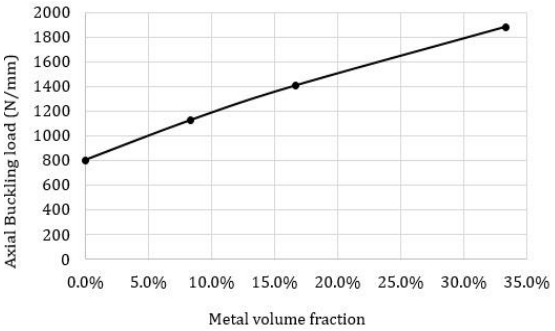

Fig. 6 Axial buckling load in terms of various volume fractions of metal

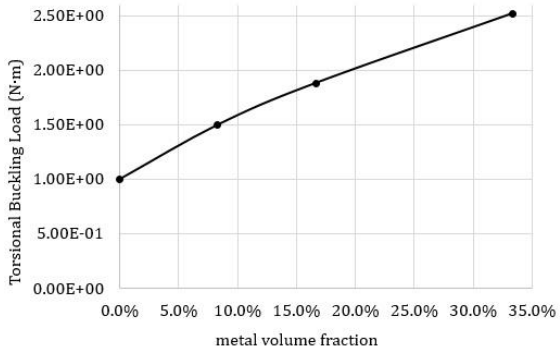

Fig. 7 Torsional buckling load in terms of various volume fractions of metal

5.4. Study of the interaction of external forces

The interaction of axial and torsional loads is investigated in this part. Figure 8 shows the interaction buckling curves of Al2024 for different metal volume fractions. While, Fig.9 shows the state of interaction of various metal types. Interaction buckling curves relate the combination of axial load and torsional load prior to buckling. N_c and T_c represent the critical axial and torsional buckling load, respectively.

It can be observed that in all cases, the curves vary almost linearly, therefore in most cases, the model shows a similar performance on the various loading configurations. Figure 8 suggests that when axial loading is more considerable, increasing the metal volume fractions leads to a decrease in buckling performance of the structure. Additionally, study of various metal types shows that Az91 and Ti6Al4V present a similar interaction behavior, whereas Al2024 lacks performance in loading cases in which the axial load is dominant.

6. Conclusions

The purpose of the present paper was to investigate the buckling behavior of FML composite cylindrical shells under different loading conditions. The Kirchhoff Love-type assumption was employed to determine the distribution of strain over the thickness. Then, the analytical formulation was presented for the state of pure axial compression loading.

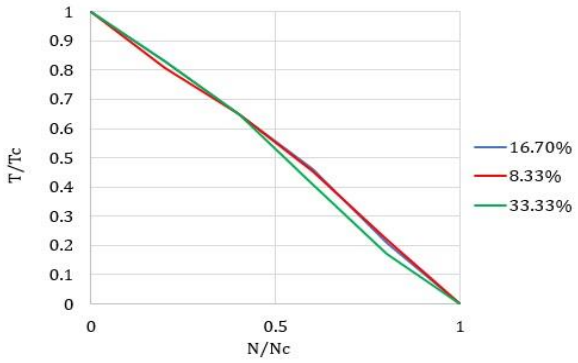

Fig. 8 The state of interaction of Al2024 for various metal volume fractions

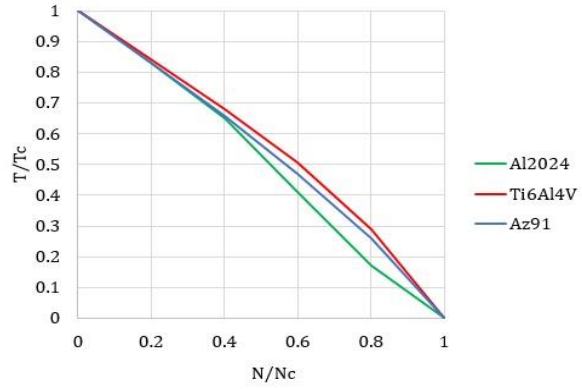

Fig. 9 The state of interaction of various metal types under axial and torsional loading

Next, various stacking sequences were considered and the optimal design of composite layers was determined using analytical solution. Also, a comprehensive FEM analysis was performed and the results were compared with analytical ones. It was established that the lay-up is the optimal layer arrangement. It was observed that the drawback of the Kirchhoff Love-type solution was the inaccurate calculation of the buckling load, particularly in cases that displayed twisting mode shapes. Another equally important parameter was the critical load to mass ratio of the cylinder. It was revealed that the Ti6Al4V and Al2024 had the highest load to mass ratio. Accordingly, it was concluded that the Al2024 was overall the best choice among the three suggested metal types. It was also clarified that addition of metal layers can noticeably enhance the buckling behavior of composite shells. The results also revealed that as the metal volume fraction raised by 15%, the endurable buckling load increased almost 43% compared to the state where there was no metal layer. The numerical results indicated that when the axial loading was more considerable, increasing the metal volume fractions led to a decrease in buckling performance of the structure. Study of various metal types showed that Az91 and Ti6Al4V presented a similar interaction behavior, whereas Al2024 lacked structural performance

in loading cases where the axial load was dominant.

References

[1]. Nayyeri Amiri S., Rasheed H.A., 2017. Nondestructive method to predict the buckling load in elastic spherical shells. Eng Struct, 150, pp.300–317. doi: 10.1016/j.engstruct.2017.07.020

[2]. Nejad M.Z., Jabbari M., Hadi A., 2017. A review of functionally graded thick cylindrical and conical shells. J Comput Appl Mech, 48, pp.357–370. doi: 10.22059/JCAMECH.2017.247963.220

[3]. Asghari B., Ghasemi A.R., Tabatabaeian A., 2019. On the optimal design of manufacturing-induced residual stresses in filament wound carbon fiber composite cylindrical shells reinforced with carbon nanotubes. Compos Sci Technol, pp.107743. doi: 10.1016/j.compscitech.2019.107743

[4]. Nejati, M., Ghasemi-Ghalebahman, A., Soltanimaleki, A., Dimitri, R., & Tornabene, F. 2019. Thermal vibration analysis of SMA hybrid composite double curved sandwich panels. Compos Struc, 224, 111035. doi:10.1016/j.compstruct.2019.111035.

[5]. Taheri-Behrooz, F., Omidi, M. 2018. Buckling of axially compressed composite cylinders with geometric imperfections. Steel and Compos Struc, 29(4), 557-567. doi: 10.12989/scs2018.29.4.557

[6]. Arefi M., Mohammadi M., Amir-ahmadi S., Rabczuk T., 2019. Thin-Walled Structures FSDT electro-elastic analysis of FG-CNTRC cylindrical three-layered pressure vessels with piezoelectric face-sheets. Thin Walled Struct. doi: 10.1016/j.tws.2019.106320

[7]. Tahir Z ul R., Mandal P., 2017. Artificial neural network prediction of buckling load of thin cylindrical shells under axial compression. Eng Struct, 152, pp.843–855. doi: 10.1016/j.engstruct.2017.09.016

[8]. Hajmohammad M.H., Tabatabaeian A., Ghasemi A.R., Taheri-Behrooz F., 2020. A novel detailed analytical approach for determining the optimal design of FRP pressure vessels subjected to hydrostatic loading : Analytical model with experimental validation. Compos Part B, 183, pp.107732. doi: 10.1016/j.compositesb.2019.107732

[9]. Geier B., Meyer-Piening H.R., Zimmermann R., 2002. On the influence of laminate stacking on buckling of composite cylindrical shells subjected to axial compression. Compos Struct, 55, pp.467–474. doi: http://dx.doi.org/10.1016/S0263-8223(01)00175-1

[10]. Tafreshi A., Bailey C.G., 2007. Instability of imperfect composite cylindrical shells under combined loading. Compos Struct, 80, pp.49–64. doi: 10.1016/j.compstruct.2006.02.031

[11]. Taheri-Behrooz F., Omidi M., Shokrieh M.M., 2017. Experimental and numerical investigation of buckling behavior of composite cylinders with cutout. Thin-Walled Struct 116, pp.136–144. doi: 10.1016/j.tws.2017.03.009

[12]. Shen H.S., Xiang Y., 2018. Postbuckling of functionally graded graphene-reinforced composite laminated cylindrical shells subjected to external pressure in thermal environments. Thin-Walled Struct, 124, pp.151–160. doi: 10.1016/j.tws.2017.12.005

[13]. Civalek Ö., 2017. Buckling analysis of composite panels and shells with different material properties by discrete singular convolution (DSC) method. Compos Struct, 161, pp.93-110.

[14]. Tabatabaeian A., Ghasemi A.R., 2019. Curvature changes and weight loss of polymeric nano-composite plates with consideration of the thermal cycle fatigue effects and different resin types: An experimental approach. Mech Mater, 131, pp.69–77. doi: 10.1016/j.mechmat.2019.01.017

[15]. Ghasemi A.R., Tabatabaeian A., Asghari B., 2019. Application of slitting method to characterize the effects of thermal fatigue, lay-up arrangement and MWCNTs on the residual stresses of laminated composites. Mech Mater, 134, pp.185–192. doi: 10.1016/j.mechmat.2019.04.008

[16]. Tabatabaeian A., Baraheni M., Amini S., Ghasemi A.R., 2019. Environmental, mechanical and materialistic effects on delamination damage of glass fiber composites: Analysis and optimization. J Compos Mater, 002199831984481. doi: 10.1177/0021998319844811

[17]. Baraheni M., Tabatabaeian A., Amini S., Ghasemi A.R., 2019. Parametric analysis of delamination in GFRP composite profiles by performing rotary ultrasonic drilling approach: Experimental and statistical study. Compos Part B Eng 172, pp.612–620. doi: 10.1016/j.compositesb.2019.05.057

[18]. Tabatabaeian A., Ghasemi A.R., Asghari B., 2019. Specification of non-uniform residual stresses and tensile characteristic in laminated composite materials exposed to simulated space environment. Polym Test, 80, pp.106147. doi: 10.1016/j.polymertesting.2019.106147

[19]. Hadigheh S.A., Kashi S., 2018. Effectiveness of vacuum consolidation in bonding fibre reinforced polymer (FRP) composites onto

concrete surfaces. Constr Build Mater, 187, pp.854–864. doi: 10.1016/j.conbuildmat.2018.07.200

[20]. Hadigheh S.A., Gravina R.J., 2016. Generalization of the Interface Law for Different FRP Processing Techniques in FRPto- Concrete Bonded Interfaces. Compos Part B. doi: 10.1016/j.compositesb.2016.01.015

[21]. Tabatabaeian A., Ghasemi A.R., 2020. The impact of MWCNT modification on the structural performance of polymeric composite profiles. Polym Bull. doi: 10.1007/s00289-019-03088-0

[22]. Ghasemi A.R., Mohandes M., 2018. Comparison between the frequencies of FML and composite cylindrical shells using beam modal function model. J Comput Appl Mech. doi: 10.22059/JCAMECH.2018.242233.189

[23]. Moniri Bidgoli A.M., Heidari-Rarani M., 2016. Axial buckling response of fiber metal laminate circular cylindrical shells. Struct Eng Mech, 57, pp.45–63. doi: 10.12989/sem.2016.57.1.045

[24]. Ghasemi A.R., Mohammadi M.M., 2016. Residual stress measurement of fiber metal laminates using incremental hole-drilling technique in consideration of the integral method. Int J Mech Sci. doi: 10.1016/j.ijmecsci.2016.05.025

[25]. Ghasemi A.R., Mohandes M., 2018. Free vibration analysis of micro and nano fiber-metal laminates circular cylindrical shells based on modified couple stress theory. Mech Adv Mater Struct, 6494, pp.1–12. doi: 10.1080/15376494.2018.1472337

[26]. Asaee Z., Taheri F., 2017. Enhancement of performance of three-dimensional fiber metal laminates under low velocity impact – A coupled numerical and experimental investigation. J Sandw Struct Mater. doi: 10.1177/1099636217740389

[27]. Banat D., Kolakowski Z., Mania R.J., 2016. Investigations of fml profile buckling and post-buckling behaviour under axial compression. Thin-Walled Struct, 107, pp.335–344. doi: 10.1016/j.tws.2016.06.018

[28]. Asaee Z., Mohamed M., Soumik S., Taheri F., 2017. Experimental and numerical characterization of delamination buckling behavior of a new class of GNP-reinforced 3D fiber-metal laminates. Thin-Walled Struct, 112, pp.208–216. doi: 10.1016/j.tws.2016.12.015

[29]. Asaee Z., Taheri F., 2018. A practical analytical model for predicting the low-velocity impact response of 3D-fiber metal laminates. Mech Adv Mater Struct. doi: 10.1080/15376494.2018.1472328

[30]. Al-Masri R., Rasheed H.A., 2018. Buckling solutions of clamped-pinned anisotropic laminated composite columns under axial compression using bifurcation approach and finite elements. Thin-Walled Struct, 123, pp.206–213. doi: 10.1016/j.tws.2017.11.022

[31]. Yang J., Dong J., Kitipornchai S., 2019. Unilateral and bilateral buckling of functionally graded corrugated thin plates reinforced with graphene nanoplatelets. Compos Struct, 209, pp.789–801. doi: 10.1016/j.compstruct.2018.11.025

[32]. Chen D., Yang J., Kitipornchai S., 2019, Buckling and bending analyses of a novel functionally graded porous plate using Chebyshev-Ritz method. Arch Civ Mech Eng, 19, pp.157–170. doi: 10.1016/j.acme.2018.09.004

[33]. Ghasemi A.R., Tabatabaeian A., Moradi M., 2018. Residual stress and failure analyses of polymer matrix composites considering thermal cycling and temperature effects based on classical laminate plate theory. J Compos Mater. doi: 10.1177/0021998318812127

[34]. Song M., Yang J., Kitipornchai S., Zhu W., 2017. Buckling and postbuckling of biaxially compressed functionally graded multilayer graphene nanoplatelet-reinforced polymer composite plates. Int J Mech Sci, 131–132, pp.345–355. doi: 10.1016/j.ijmecsci.2017.07.017

[35]. Chen D., Yang J., Kitipornchai S., 2015. Elastic buckling and static bending of shear deformable functionally graded porous beam. Compos Struct, 133, pp.54–61. doi: 10.1016/j.compstruct.2015.07.052

[36]. Inagaki I., Tsutomu T., Yoshihisa S., Nozomu A., 2014. Application and Features of Titanium for the Aerospace Industry. Nippon steel sumitomo. Met Tech Rep, pp.22–27

[37]. Mordike B.L., Ebert T., 2001. Magnesium Properties - applications - potential. Mater Sci Eng A, 302, pp.37–45. doi: 10.1016/S0921-5093(00)01351-4

[38]. Vlot A., Kroon E., La Rocca G., 1998. Impact Response of Fiber Metal Laminates. Key Eng Mater, 141–143, pp.235–276. doi: 10.4028/www.scientific.net/KEM.141-143.235